# Tangential flow filtration for continuous processing of crystallized proteins

Ali Behboudi\*, Mirko Minervini, Alexander Kedzierski, Lawrence Azzariti, Andrew L. Zydney\*

Department of Chemical Engineering The Pennsylvania State University University Park, PA 16802

#### Submitted to

## **Separation and Purification Technology**

\*Corresponding authors:

Andrew Zydney — <u>zydney@engr.psu.edu</u> Ali Behboudi — <u>aub793@psu.edu</u>

#### Abstract

Protein crystallization has the potential to provide nearly pure protein products in a single processing step. Most previous studies of protein crystallization have used centrifugation for dewatering and washing the crystallized solids, but this approach would be difficult to adopt in continuous bioprocessing operations. This study provides the first demonstration that crystallized proteins can be successfully filtered using hollow fiber tangential flow filtration (TFF) modules. Experiments were performed with human serum albumin (HSA) crystallized by the addition of trivalent CeCl<sub>3</sub>, both with and without polyethylene glycol (PEG). Greater than 85% protein yield was achieved using 4.5 mM CeCl<sub>3</sub> in the presence of 3 wt.% PEG with the crystallization occurring in less than 20 s, which is ideal for continuous processing. The addition of PEG had minimal effect on the crystallization yield, but it did lead to the formation of larger and denser crystals and a corresponding increase in the critical flux, which is the maximum value of the flux that causes minimal increase in the transmembrane pressure (i.e., minimal fouling). Filtration experiments performed at optimal conditions were successfully run for 24 hours with the transmembrane pressure remaining below 5 kPa demonstrating the feasibility of using continuous crystallization with tangential flow filtration for the purification of high value protein products.

**Keywords**: protein crystallization, human serum albumin, tangential flow filtration, continuous processing

#### 1. Introduction

The potential for using crystallization for protein purification and formulation has been recognized for more than 100 years [1]. The regular lattice of the protein crystal can exclude a wide range of impurities, including misfolded versions of the desired protein product. One of the final steps in the manufacture of recombinant human insulin is crystallization, typically induced by the addition of Zn [2]. A number of recent studies have demonstrated the feasibility of using crystallization for the purification and concentration of monoclonal antibodies, which are currently the dominant class of biopharmaceuticals [3]. For example, Zang et al. showed more than 95% exclusion of model protein impurities during the crystallization of an IgG4 monoclonal antibody in micro-batch (60 well plate) crystallizers [4]. Smejkal et al. examined the crystallization of an IgG1 monoclonal antibody up to 1 L scale, with successful crystallization from a clarified and conditioned cell culture fluid [5]. Although there have been no detailed economic assessments of large-scale protein crystallization as an alternative to chromatographic separations, the ability to perform crystallization in simple stirred tanks or continuous tubular plug-flow crystallizers could dramatically reduce manufacturing costs [6].

Previous studies of protein crystallization have performed the dewatering / washing of the crystals by batch centrifugation [4, 5] or by dead-end (typically vacuum) filtration [7]. Cornehl et al. were able to process lysozyme crystals using a small stirred cell filter, although this system would be difficult to operate at a large scale [8]. However, none of these approaches would be attractive in the context of continuous bioprocessing, which has been a major focus for lower cost biomanufacturing operations [9]. There have been several efforts to develop continuous crystallization + filtration processes for the pharmaceutical industry, although these have not yet been applied in commercial manufacturing. For example, Domokos et al. [10] used a carousel of Nutsche (normal flow) filtration units to process crystals of acetylsalicylic acid. Although the system could be operated continuously, the individual filtration units operated in a batch mode due to the time-dependent growth of a filter cake composed of packed crystals [10]. Steenweg et al.

used a continuous vacuum screw filter for processing crystallized L-alanine, with stable operation achieved for up to one hour [11].

A potentially more attractive approach for the continuous processing of protein crystals is tangential flow filtration (TFF). TFF is already used extensively in commercial bioprocessing, both for initial clarification and final formulation [12]. Several recent studies have demonstrated that TFF can also be used for dewatering and washing precipitated proteins, including human serum immunoglobulin [13] and monoclonal antibodies [14]. The key is to operate the TFF device below the critical flux, which is the maximum value of the filtrate flux that provides stable operation with minimal fouling (as denoted by a nearly constant transmembrane pressure during constant flux operation). However, we are not aware of any prior studies on the application of TFF for the processing of crystallized proteins.

The work described in this paper provides the first examination of TFF for protein crystals, using human serum albumin (HSA) crystallized with Cerium (III) chloride (CeCl<sub>3</sub>) as a model system based on the recent work by Buchholz et al. [15]. The critical flux was evaluated using flux-stepping experiments to identify conditions that could provide long-term stable operation of the TFF system. Operation of the hollow fiber module below the critical flux enabled continuous filtration for 24 hr with the transmembrane pressure remaining below 5 kPa. These results clearly demonstrate the potential of using TFF for the development of a continuous crystallization + filtration process for protein purification or formulation.

#### 2. Materials and Methods

Lyophilized human serum albumin (HSA) was purchased from NovaBiologics and stored at 4°C until use. HEPES (4-(2-hydroxyethyl)-1-piperazineethanesulphonic acid) and TRIS-HCl were used as buffers. Cerium (III) chloride (CeCl<sub>3</sub>, AnhydroBeads™, −10 mesh, ≥99.99% trace metals basis, SKU 429406) and polyethylene glycol (202444, Mn ~ 3350) were used to control protein solubility and cause crystallization. All chemicals were purchased from Millipore Sigma. Filtration experiments were performed

using Reuse-Line modified polyether sulfone (m-PES) hollow fiber membranes with a different pore sizes (0.1, 0.2, and 0.45 μm), lengths (30 and 60 cm), and surface area (51.8, 106, and 155 cm<sup>2</sup>), all obtained from Sartorius.

## 2.1. Protein crystallization and characterization

Effective crystallization conditions were identified using small batch crystallization experiments performed by dissolving different concentrations of HSA in the appropriate buffer at pH 7, with the buffer pH adjusted by the addition of 5 M HCl as needed. CeCl<sub>3</sub>, and in some cases, PEG, were then added to induce crystallization. 5 mL of the HSA solution was mixed with an equal volume of the CeCl<sub>3</sub> / PEG solution in a 15 ml tube to produce 10 ml of the crystallization solution. Samples were taken periodically and centrifuged at 8000 rpm and 4°C using an Eppendorf 5415 R centrifuge. The supernatant was carefully collected to measure the concentration of dissolved (uncrystallized) protein. The crystal yield was evaluated as:

$$Y(\%) = (1 - \frac{c_s}{c_t}) \times 100 \tag{1}$$

where  $C_s$  and  $C_t$  are the HSA concentrations in the collected supernatant and the overall solution, respectively.

Larger scale crystallization was performed using a tubular flow reactor fitted with static mixers (Koflo Corporation, Cary, IL). This system provides very uniform residence time, which is particularly attractive for continuous bioprocessing for protein therapeutics. The tubular reactor consists of 3 static mixer units of 20 cm long each with 24 helical subunits of static mixer plus another 10 cm of empty tubing for material transfer summing up to 70 cm of total length. The buffered HSA solution and the CeCl<sub>3</sub> / PEG solution were both fed to the crystallizer via a Y-connector at flow rates of 10 mL/min giving a total residence time of 60 s in the plug flow crystallizer.

HSA crystals were examined by optical microscopy using a DMi8 Thundered Microscope (Leica). 3D binarized images were constructed using a z-axis shift through a field of view. Image processing software (ImageJ) was used to evaluate the particle size distribution (PSD) and the fractal dimension, with the latter determined using the Box Count app in MATLAB (R2022 b).

Protein secondary structure for the native HSA and for the crystallized protein after redissolution in 2.5 mM TRIS at pH 7 were examined by circular dichroism (CD) using a Jasco J-1500 spectrometer with quartz cells and a xenon arc lamp source. Three spectra were obtained for each sample and averaged, with baseline correction performed using the spectra for the corresponding buffer (TRIS alone for the native HSA and TRIS plus CeCl<sub>3</sub> for the crystallized protein).

## 2.2. Flux-stepping experiments

Sustainable filtration conditions for dewatering the crystallized HSA were evaluated from flux-stepping experiments [14, 16], which is a well-established method for identifying TFF conditions that have minimal fouling. The crystallized HSA solution was fed to the lumen side of the hollow fiber membrane using a peristaltic pump at flow rates from 10, to 40 mL/min. The permeate flow rate (at fixed feed flow rate) was increased in a stepwise fashion using a pump on the permeate exit line. The inlet feed  $(P_F)$ , exit retentate  $(P_R)$ , and permeate  $(P_P)$  pressures were evaluated using Ashcroft digital pressure gauges, with the transmembrane pressure (TMP) evaluated as:

$$TMP = \frac{P_F + P_R}{2} - P_P \tag{3}$$

Filtration was continued until the TMP became unstable, i.e., until the increase in TMP with time during the constant flux filtration was > 0.2 kPa/h. At the end of each experiment, the hollow fiber membrane module was flushed with buffer and then cleaned using a 0.5 M NaOH solution at 40 °C for 30 min.

#### 3. Results and Discussion

## 3.1. Crystallization

Several recent studies have examined the crystallization and overall phase behavior of HSA in the presence of CeCl<sub>3</sub> [15, 17, 18]. The trivalent Ce<sup>3+</sup> ions bind to the negatively charged HSA, minimizing electrostatic repulsion and increasing the net hydrophobic attraction leading to liquid-liquid phase separation and crystal formation. Typical contour plots for the crystallization yield as a function of the HSA and CeCl<sub>3</sub> concentrations are shown in Figure 1 for HSA in DI water (top panel) and HSA in HEPES and TRIS buffers (lower two panels), all at pH 7. The degree of crystallization was fairly low under most conditions with DI water, although a solution with 50 g/L HSA and ≈5 mM CeCl<sub>3</sub> gave a crystal yield of nearly 80%. However, the crystalline phase generated under these conditions appeared "gel-like" and was not able to be processed by TFF. Further increases in the CeCl<sub>3</sub> concentration appeared to disrupt the phase separation and reduce the yield.

HSA crystallization from 50 mM HEPES and TRIS was much more effective, particularly at low HSA and CeCl<sub>3</sub> concentrations (shown by the blue circles) than crystallization from water. The maximum yield of 83 ± 4% was obtained with a TRIS buffer using 5 g/l HSA and 3 mM CeCl<sub>3</sub>, although a yield of above 82.1% could be achieved at HSA concentrations as high as 25 g/L using 8 mM CeCl<sub>3</sub> (Figure 1). The crystals formed at HSA concentrations below 10 g/L remained well suspended, but the solution became viscous and gel-like at higher protein and CeCl<sub>3</sub> concentrations. A slightly higher yield (86 ± 3%) could be obtained by the addition of PEG, which acts as a volume exclusion agent that facilitates both protein crystallization and precipitation [3]. The crystallization yield was only weakly dependent on the PEG concentration from 0 to 12% PEG by weight (data not shown). In both cases, the crystallization occurred rapidly (in less than 10 s), with the crystal yield in the tubular crystallizer nearly identical to that obtained in the small-scale batch crystallization experiments.

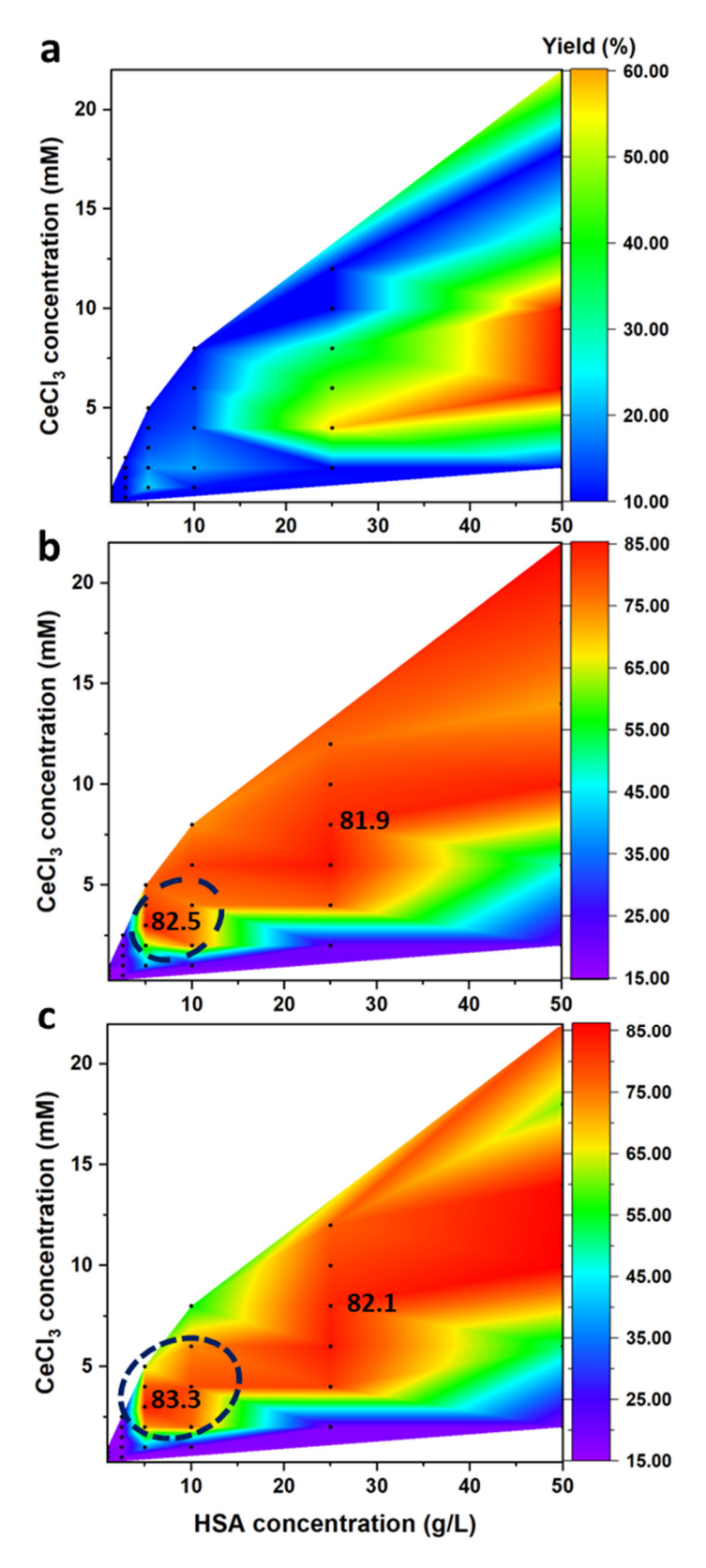
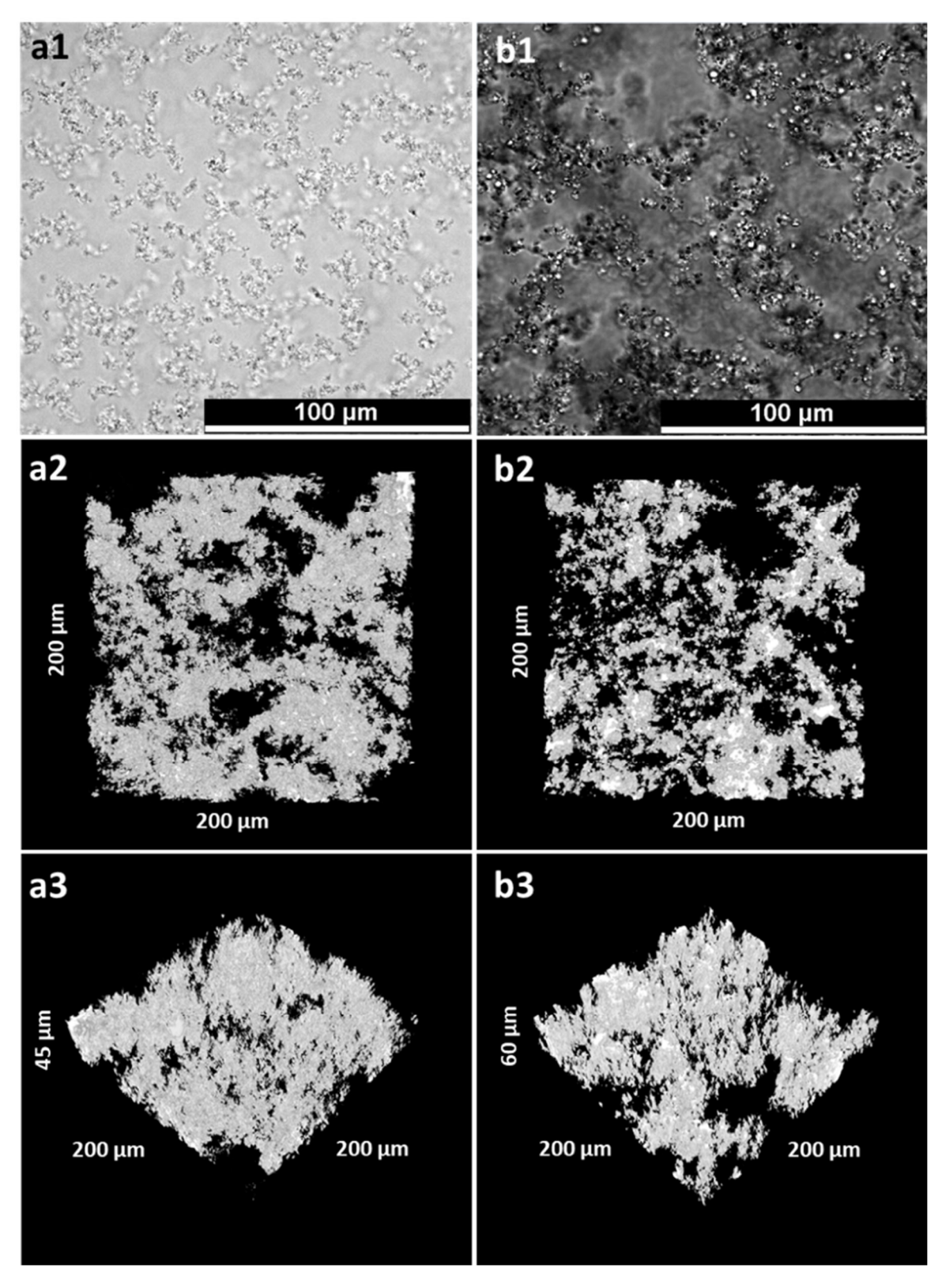


Figure 1 - Crystallization yield as a function of the HSA and  $CeCl_3$  concentrations in (a) DI water, (b) HEPES, and (c) TRIS buffers.

The morphology of the HSA crystals formed from 5 g/L solutions of HSA in 50 mM TRIS with 4.5 mM CeCl<sub>3</sub>, both with and without 3% PEG, are shown in Figure 2. The addition of PEG resulted in larger particles with more spherical shapes and a highly dense core (the more pronounced white center of the particles in the right-hand panels).



**Figure 2** - Microscopic images of crystallized HSA formed from 5 g/l HSA solutions in TRIS with 4.5 mM CeCl<sub>3</sub>, both alone (left panels) and in the presence of 3% PEG. (1) raw 2D images, (2) 2D bright field view, and (3) 3D reconstructions.

The effect of PEG on the particle size is shown more clearly in Figure 3, with the size distributions determined based on the analysis of more than 2500 particles under each crystallization condition. The average particle size increased from 9.3 to 17 µm upon the addition of PEG, with the fractal dimension increasing from 2.40 to 2.77. Pons Royo et al. showed that there is a positive correlation between smaller fractal dimensions and the formation of precipitates with reduced compactness and durability [19]. Precipitates with greater fractal dimension typically show better resistance to shear break-up [20, 21] and improved filtration performance in batch filtration systems [22, 23].

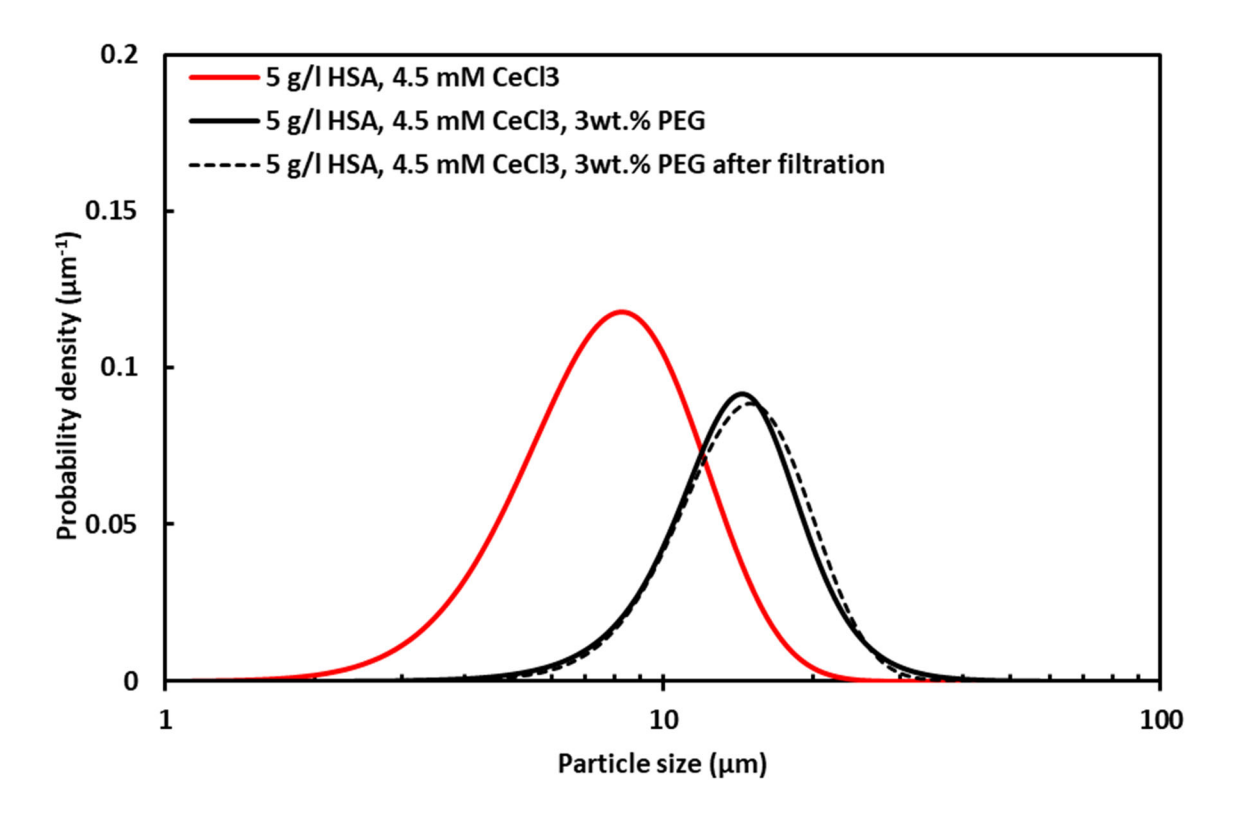


**Figure 3** - Effect of PEG on the particle size distributions for crystallized HSA in TRIS with 4.5 mM CeCl<sub>3</sub>, both alone and in the presence of 3% PEG. The dashed curve is for the crystallized HSA at the end of the tangential flow filtration experiment.

Figure 4 shows the CD spectra of the native HSA, prepared by dissolving the lyophilized protein directly in a TRIS buffer, and the HSA crystals prepared with CeCl<sub>3</sub> alone and with CeCl<sub>3</sub> + 3 wt % PEG,

both after resolublization in TRIS. The CD spectra is highly sensitive to the protein secondary structure, including both the alpha helix and beta sheet content [24]. The curves for the native and resolublized protein are nearly identical; the negative bands at 208 and 222 nm are both characteristic of the alpha helical structure. The absence of any structural changes in the protein upon crystallization has also been demonstrated with multiple monoclonal antibodies. For example, Yang et al. [25] demonstrated that crystallized rituximab, trastuzumab, and infliximab all retain full biological activity after batch crystallization.

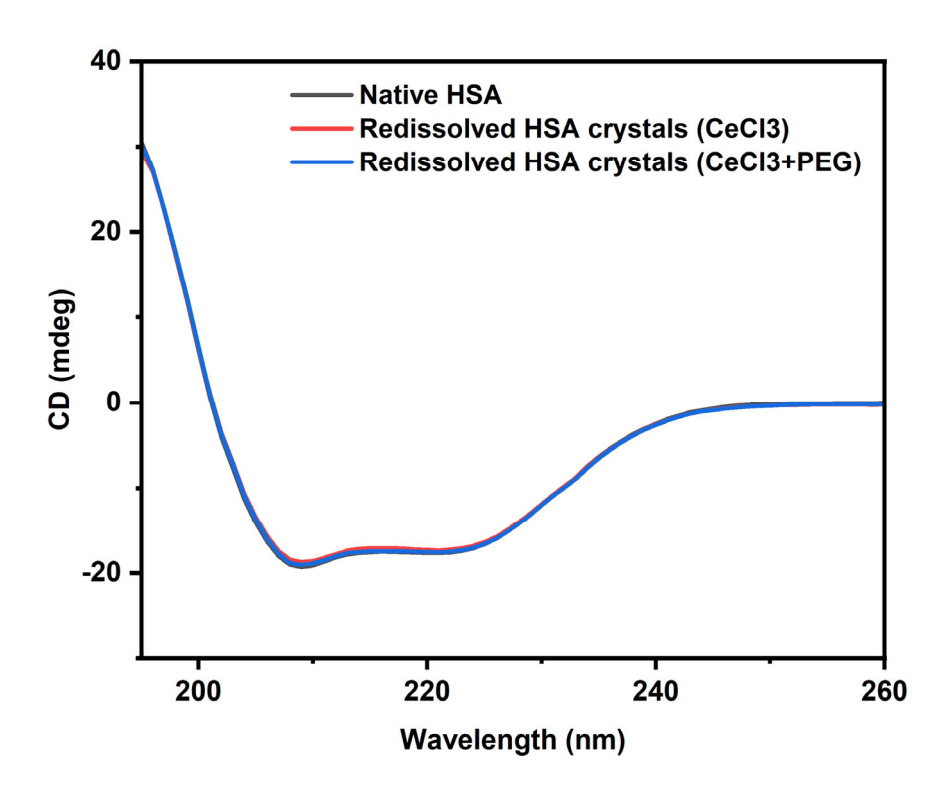


**Figure 4** - Circular dichroism spectra of native HSA and redissolved HSA crystals formed with 4.5 mM CeCl<sub>3</sub> alone and with 4.5 mM CeCl<sub>3</sub> + 3 wt % PEG.

## 3.2. Flux-stepping experiments

Figure 5 shows results from flux-stepping experiments performed with crystallized HSA obtained from 5 g/L HSA solutions with 4.5 mM CeCl<sub>3</sub>. The data were obtained with 0.2 µm pore size hollow fiber membrane modules with a length of 30 cm (giving a total filtration area of 155 cm<sup>2</sup>) at a feed flow rate of

20 mL/min. This corresponds to an inlet wall shear rate of 210 s<sup>-1</sup> assuming Poiseuille flow. The top panel shows results for crystals formed in the absence of PEG. There was no measurable difference in the particle size distribution or morphology for crystal samples examined before and after the flux-stepping experiment, suggesting that there was no shear-induced crystal breakage under these conditions. The TMP remained stable during operation at the first four values of the filtrate flux, but then increased from 2.3 to 6.0 kPa (0.33 to 0.87 psi) over 25 min of filtration at a flux of 30.9 L/m<sup>2</sup>/h (8.6  $\mu$ m/s). The maximum sustainable flux was evaluated as the average of the filtrate flux values just above and below the stable TMP, giving a critical flux of 29 ± 2 L/m<sup>2</sup>/h under these conditions.

The middle panel of Figure 5 shows corresponding data obtained for HSA crystallized in the presence of 3% PEG. In this case, operation at  $30.9 \text{ L/m}^2/\text{h}$  gave a completely stable TMP. The TMP began to show a small increase during filtration at  $34.7 \text{ L/m}^2/\text{h}$ , but the TMP gradient was much less than 0.2 kPa/h (0.03 psi/h), which was taken as the maximum acceptable gradient based on the work by Minervini et al. [16]. The critical flux was not reached until  $41 \pm 2 \text{ L/m}^2/\text{h}$ , which is 40% greater than that in the absence of PEG. Samples of the HSA crystals obtained at the end of the flux-stepping experiment showed nearly identical size distribution as the fresh (unfiltered) crystals (dashed curve in Figure 3) suggesting that there was no crystal breakage or aggregation in either the hollow fiber module or the peristaltic pump under these conditions.

In order to determine if the increase in critical flux was due to a change in the crystal properties or to the effects of PEG on the flow, a third experiment was performed in the HSA was crystallized in the absence of PEG but was then spiked with PEG after the crystallization was complete to give a solution containing the same concentrations of HSA, CeCl<sub>3</sub>, and PEG. The flux-stepping results are shown in the bottom panel of Figure 4, with the addition of PEG providing a small increase in the critical flux compared to the HSA and CeCl<sub>3</sub> alone (from  $29 \pm 2$  to  $32 \pm 2$  L/m<sup>2</sup>/h). This increase in critical flux occurred even though the PEG should cause a small increase in the viscosity of the solution. Instead, it is likely that the PEG reduces interactions between the crystals and the membrane surface, resulting in a lower fouling

propensity [26, 27]. The exit retentate pressure remained at approximately atmospheric under all conditions, with the inlet pressure for last flux step increasing from 1.03 to 1.17 kPa in Figures 4a and c and from 1.71 to 1.82 kPa in Figure 4b. The lack of any significant increase in the inlet feed pressure, despite the large increase in TMP, indicates that membrane fouling at high filtrate flux was due primarily to interactions with the membrane surface and not to clogging of the hollow fiber lumens [16].

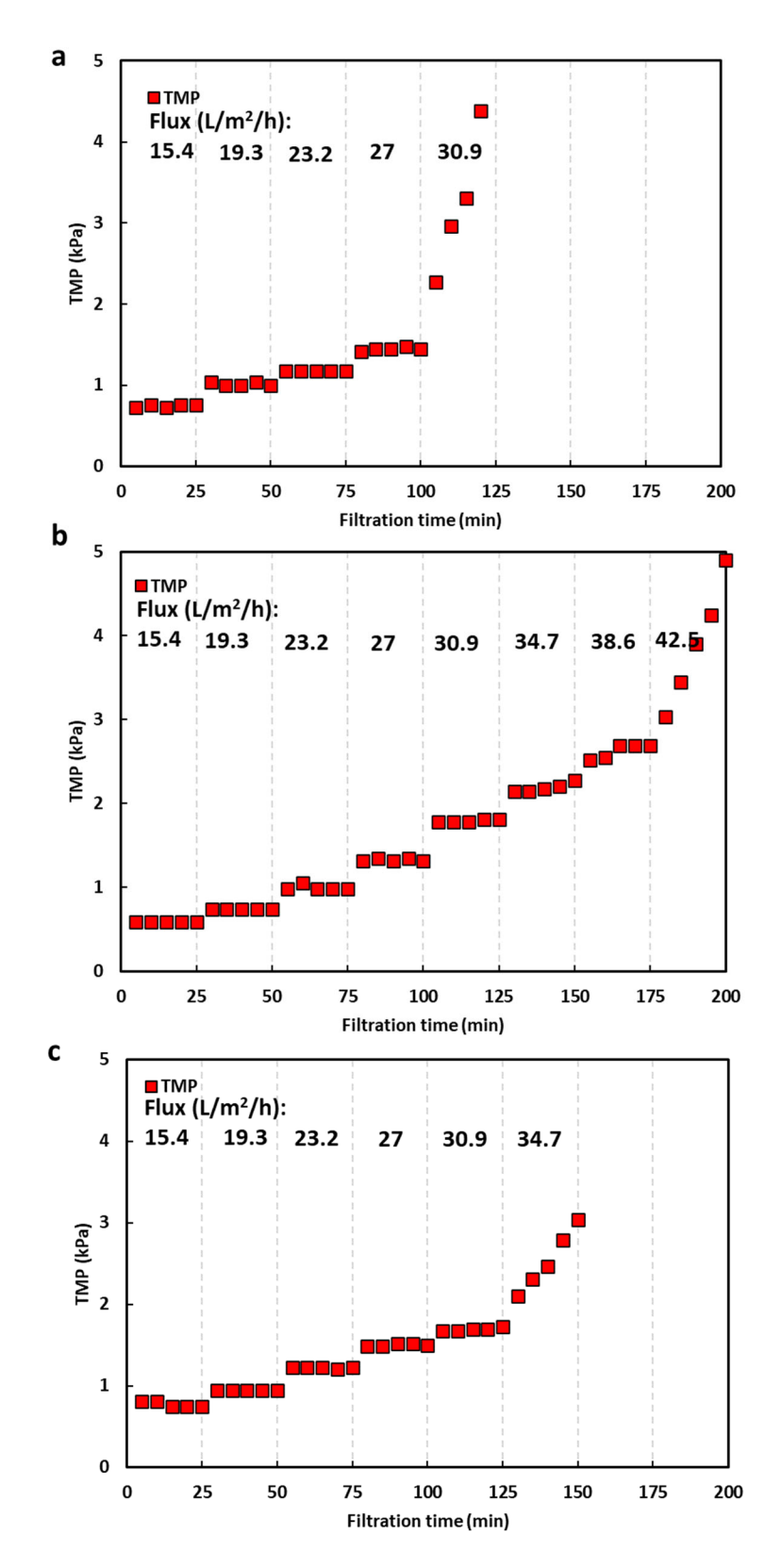


**Figure 5** - Flux-stepping experiments performed with 0.2 μm pore size hollow fiber membranes with 155 cm² area at a feed flow rate of 20 mL/min for (a) crystallized HSA, (b), HSA crystallized in the presence of 3% PEG, and (c) crystallized HSA with PEG added after the crystallization.

Additional insights into the filtration behavior for the crystallized HSA were obtained by performing flux-stepping experiments with hollow fiber membranes having pore sizes of 0.1 and 0.45  $\mu$ m, all using the 5 g/L HSA crystallized with 4.5 mM CeCl<sub>3</sub> and 3% PEG. The 0.1  $\mu$ m pore size membrane had a critical flux of 37  $\pm$  2 L/m²/h, which is 10% less than that for the 0.2  $\mu$ m membrane (Figure 5b). Interestingly, this membrane also showed some evidence of fiber clogging when operated at a flux of 38.6 L/m²/h as indicated by an increase in the feed pressure. The critical flux with the 0.45  $\mu$ m pore size membrane was 44  $\pm$  2 L/m²/h, which is slightly higher than that observed with the 0.2  $\mu$ m pore size membrane, but the permeate obtained under these conditions showed low levels of HSA, possibly due to the presence of small particles that are able to pass through the membrane pores.

In contrast to the weak dependence of the critical flux on the membrane pore size, the critical flux increased significantly with increasing shear rate with results summarized in Figure 6. All experiments were performed with the same hollow fiber module, with the membranes cleaned between experiments using 0.5 N NaOH. The critical flux increased from  $29 \pm 2$  L/m²/h at a shear rate of 110 s<sup>-1</sup> (feed flow rate of 10 ml/min) to  $71 \pm 2$  L/m²/h at 320 s<sup>-1</sup>. The data are reasonably well-described by a linear relationship, although the slope of the first 3 data points is clearly less than that for the data at high shear rates. Fitting the data to a power law relationship:

$$J_{crit} = a\gamma^n \tag{2}$$

gives  $n = 0.9 \pm 0.2$ , which is similar to the n = 1 behavior predicted by the shear-enhanced diffusion concentration polarization model [28]. It was not possible to operate these modules at even higher shear rates due to an increase in protein loss in the permeate. For example, a flux-stepping experiment performed at  $420 \text{ s}^{-1}$  showed  $\approx 7\%$  protein yield loss due to the generation of small crystal fragments at high shear rates in the hollow fiber modules and/or in the peristaltic pump used to drive the feed.

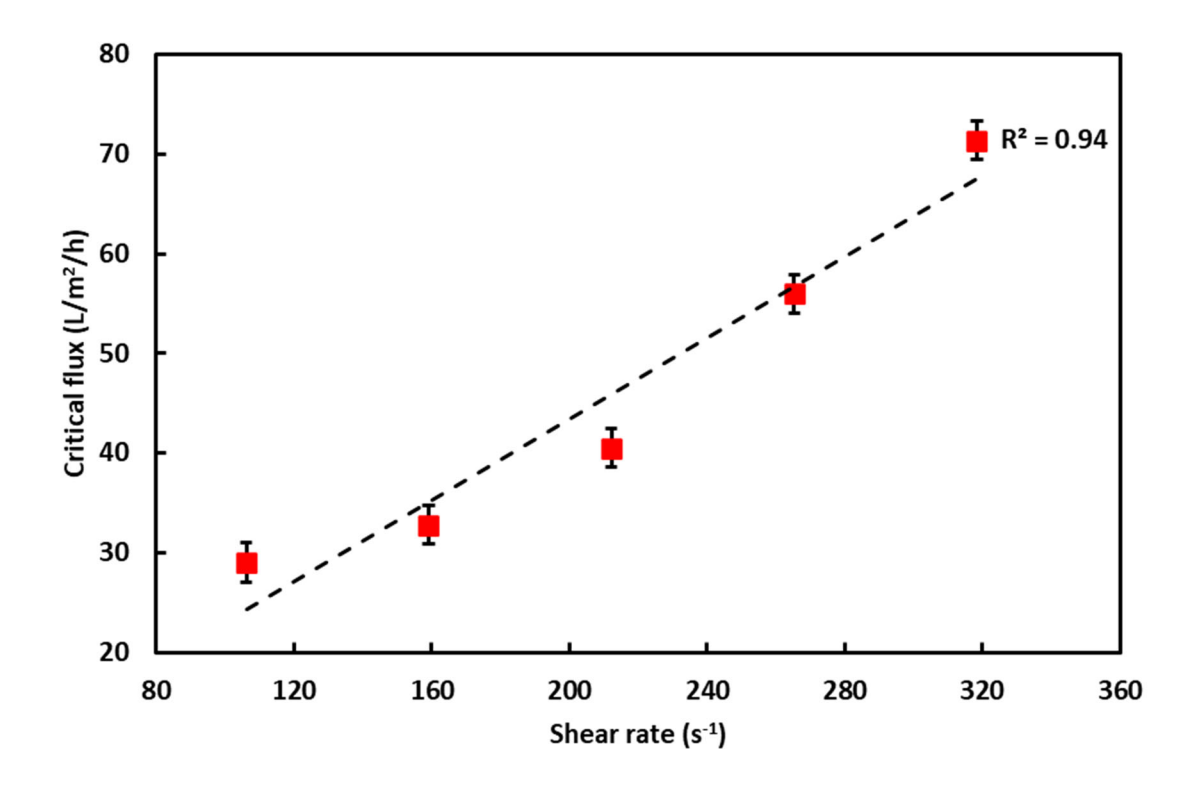


Figure 6 – Effect of inlet shear rate on the critical flux for crystals generated with 4.5 mM CeCl<sub>3</sub> and 3% PEG using 30 cm hollow fiber membranes with 0.2  $\mu$ m pore size and 155 cm<sup>2</sup> membrane area.

Limited experiments were also performed to examine the effect of fiber length on the critical flux. Data were obtained with the 30 and 60 cm modules, each with 8 fibers (giving surface areas of 52 and 106 cm<sup>2</sup>) at the same flow rate of 20 ml/min. The critical flux for the 30 cm fiber was  $64 \pm 2$  L/m<sup>2</sup>/h compared to  $43 \pm 2$  L/m<sup>2</sup>/h in the 60 cm fiber. In addition, the pressure profiles in the longer module showed clear evidence of fiber clogging. This behavior may be related to the greater pressure drop due to flow through the longer fibers, which leads to a larger local transmembrane pressure drop at the fiber inlet. Additional studies will be required to identify the underlying physical phenomena governing this behavior more fully.

## 3.3. Long-run experiments

In order to confirm that it was possible to use the hollow fiber modules for long-term filtration of the crystallized protein, an experiment was performed using the  $155 \, \mathrm{cm^2}$  module at a feed flow rate of 30 mL/min (shear rate of  $320 \, \mathrm{s^{-1}}$ ) operated at a filtrate flux of  $65 \, \mathrm{L/m^2/h}$  using HSA crystallized from a  $5 \, \mathrm{g/L}$  solution with  $4.5 \, \mathrm{mM} \, \mathrm{CeCl_3}$  and  $3\% \, \mathrm{PEG}$ . The chosen filtrate flux is slightly lower than the critical flux of  $71 \pm 2 \, \mathrm{L/m^2/h}$  obtained under these conditions. As shown in Figure 7, the TMP remained below  $5 \, \mathrm{kPa}$  (<1 psi) throughout the 24-hour filtration, with a TMP gradient of less than  $0.15 \, \mathrm{kPa/hr}$ . Note that it would take more than  $1000 \, \mathrm{hr}$  of continuous operation for the TMP to exceed  $150 \, \mathrm{kPa}$  if this TMP gradient were maintained throughout the filtration, clearly demonstrating the potential of using tangential flow filtration for continuous processing of crystallized proteins. Also shown for comparison in Figure 6 are data obtained with the same module under identical operating conditions with HSA crystallized using  $4.5 \, \mathrm{mM} \, \mathrm{CeCl_3}$  but without any added PEG. In this case, the TMP exceeded  $10 \, \mathrm{kPa}$  within  $5 \, \mathrm{min}$  of operation, consistent with the use of an operating flux ( $65 \, \mathrm{L/m^2/h}$ ) that is above the critical flux for the HSA crystals formed without the added PEG ( $48 \, \mathrm{L/m^2/h}$ ).

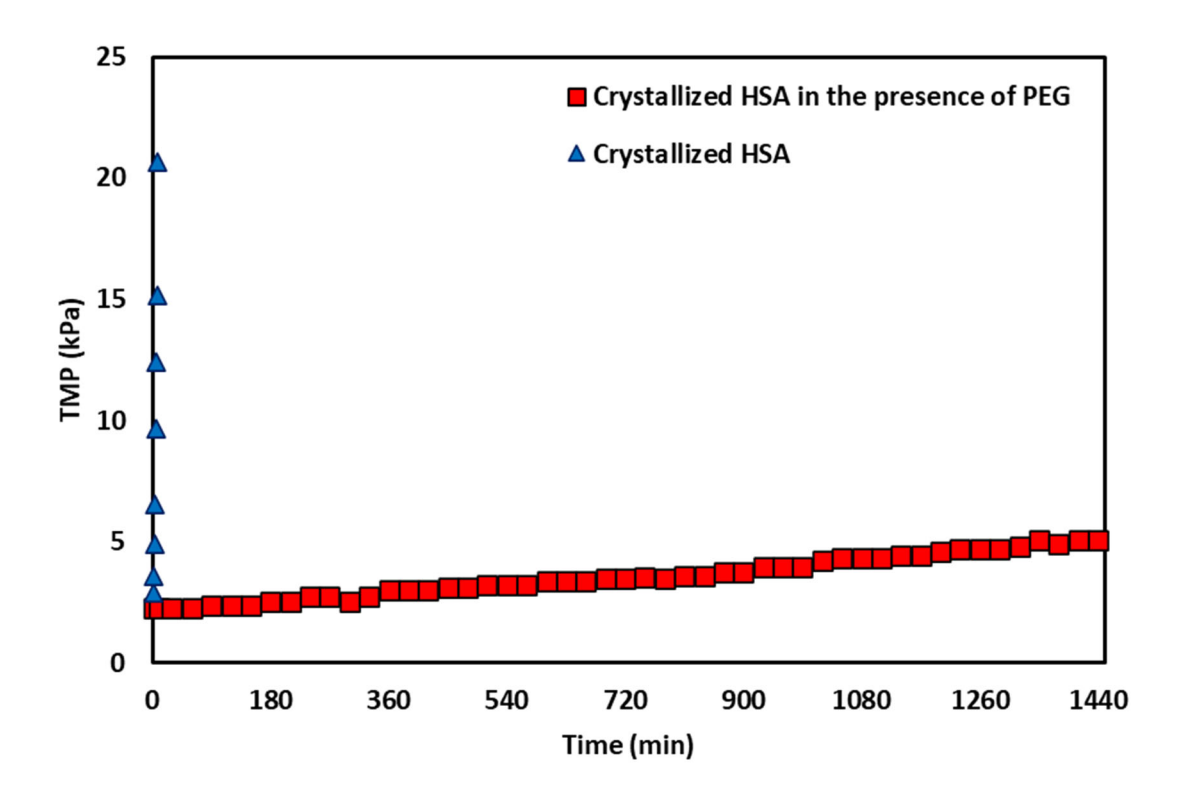


Figure 7 – Long-time filtration experiments performed using 0.2 μm hollow fiber membranes with 155 cm² area at a feed flow rate of 30 mL/min (shear rate of 320 s⁻¹) and a constant filtrate flux of 65 L/m²/h for crystallized HSA formed using 4.5 mM CeCl₃ both with and without 3% PEG.

## Conclusion

This study provided the first demonstration that tangential flow filtration can be successfully employed for dewatering of crystallized proteins using human serum albumin as a model protein. HSA was rapidly crystallized (<20 s) at high yield (>80%) using very small quantities of trivalent Ce<sup>+3</sup> (4.5 mM) in TRIS buffer at low HSA concentrations (5 g/L), which could be attractive as an alternative method for purification/formulation of albumin therapeutics. Interestingly, the addition of PEG not only provided a small increase in yield (up to 86%), but also significantly improved the filterability of the crystals by changing the particle morphology and size distribution. The crystallization had no effect on the secondary structure of the HSA as demonstrated by circular dichroism.

Flux-stepping experiments were used to identify the critical flux for the sustainable operation of

the TFF device. The critical flux increased with increasing shear rate to a value of  $71 \pm 2$  L/m<sup>2</sup>/h at a shear

rate of 320 s<sup>-1</sup>. It was possible to operate the TFF module for 24 hours at a flux slightly below this critical

flux - with a TMP gradient of <0.15 kPa/hr, suggesting that it would be possible to perform a continuous

filtration for as much as 1000 hr (40 days). Operation at higher shear rates (>400 s<sup>-1</sup>) appeared to cause

crystal breakage, while the use of longer hollow fibers led to fiber clogging. Future studies will be required

to evaluate the effectiveness of crystallization for protein purification and to develop more detailed

descriptions of the physical phenomena controlling the filtration behavior and its relationship to the

underlying crystal morphology and particle size distribution.

**CRediT** authorship contribution statement

Ali Behboudi: Conceptualization, Investigation, Data curation, Writing - original draft.

Mirko Minervini: Data curation, Investigation, Writing – original draft.

Alexander Kedzierski: Investigation, Data curation, Writing – original draft.

Lawrence Azzariti: Investigation, Data curation, Writing – original draft.

Andrew L. Zydney: Conceptualization, Funding, Supervision, Writing - review & editing

**Declaration of competing interest** 

The authors declare that they have no known competing financial interests or personal relationships that

could have appeared to influence the work reported in this paper.

Data availability

Data will be made available on request.

Acknowledgments

The work was supported by a contract from the U.S. FDA PMQWP 324, The authors would like to thank

A. Sheikhi for access to the Leica microscope.

Disclaimer

20

This report was prepared as an account of work sponsored by an agency of the United States Government. Neither the United States Government nor any agency thereof, nor any of their employees, makes any warranty, express or implied, or assumes any legal liability or responsibility for the accuracy, completeness, or usefulness of any information, apparatus, product, or process disclosed, or represents that its use would not infringe privately owned rights. Reference herein to any specific commercial product, process, or service by trade name, trademark, manufacturer, or otherwise does not necessarily constitute or imply its endorsement, recommendation, or favoring by the United States Government or any agency thereof. The views and opinions of authors expressed herein do not necessarily state or reflect those of the United States Government or any agency thereof.

#### References

- [1] D. Hekmat, Large-scale crystallization of proteins for purification and formulation, Bioprocess and Biosystems Engineering, 38 (2015) 1209-1231.
- [2] D. Roush, M. Iammarino, R. Chmielowski, F. Insaidoo, M.A. McCoy, A. Ortigosa, M. Rauscher, Insulin purification—Innovation continuum via synthesis of fundamentals, technology, and modeling, Biotechnology and Bioengineering, n/a.
- [3] W. Chen, X. Li, M. Guo, F.J. Link, S.S. Ramli, J. Ouyang, I. Rosbottom, J.Y.Y. Heng, Biopurification of monoclonal antibody (mAb) through crystallisation, Separation and Purification Technology, 263 (2021) 118358.
- [4] Y. Zang, B. Kammerer, M. Eisenkolb, K. Lohr, H. Kiefer, Towards Protein Crystallization as a Process Step in Downstream Processing of Therapeutic Antibodies: Screening and Optimization at Microbatch Scale, PLOS ONE, 6 (2011) e25282.
- [5] B. Smejkal, N.J. Agrawal, B. Helk, H. Schulz, M. Giffard, M. Mechelke, F. Ortner, P. Heckmeier, B.L. Trout, D. Hekmat, Fast and scalable purification of a therapeutic full-length antibody based on process crystallization, Biotechnology and Bioengineering, 110 (2013) 2452-2461.
- [6] P. Neugebauer, J.G. Khinast, Continuous Crystallization of Proteins in a Tubular Plug-Flow Crystallizer, Crystal Growth & Design, 15 (2015) 1089-1095.
- [7] J. Hubbuch, M. Kind, H. Nirschl, Preparative Protein Crystallization, Chemical Engineering & Technology, 42 (2019) 2275-2281.
- [8] B. Cornehl, T. Grünke, H. Nirschl, Mechanical Stress on Lysozyme Crystals during Dynamic Cross-Flow Filtration, Chemical Engineering & Technology, 36 (2013) 1665-1674.
- [9] A.L. Zydney, Continuous downstream processing for high value biological products: A Review, Biotechnology and Bioengineering, 113 (2016) 465-475.
- [10] A. Domokos, B. Nagy, M. Gyürkés, A. Farkas, K. Tacsi, H. Pataki, Y.C. Liu, A. Balogh, P. Firth, B. Szilágyi, G. Marosi, Z.K. Nagy, Z.K. Nagy, End-to-end continuous manufacturing of conventional compressed tablets: From flow synthesis to tableting through integrated crystallization and filtration, International Journal of Pharmaceutics, 581 (2020) 119297.
- [11] C. Steenweg, A.C. Kufner, J. Habicht, K. Wohlgemuth, Towards Continuous Primary Manufacturing Processes— Particle Design through Combined Crystallization and Particle Isolation, Processes, 9 (2021) 2187.
- [12] R. van Reis, A. Zydney, Membrane separations in biotechnology, Current Opinion in Biotechnology, 12 (2001) 208-211.
- [13] G. Dutra, D. Komuczki, A. Jungbauer, P. Satzer, Continuous capture of recombinant antibodies by ZnCl2 precipitation without polyethylene glycol, Engineering in Life Sciences, 20 (2020) 265-274.
- [14] M. Minervini, M. Mergy, Y. Zhu, M.A. Gutierrez Diaz, C. Pointer, O. Shinkazh, S.F. Oppenheim, S.M. Cramer, T.M. Przybycien, A.L. Zydney, Continuous precipitation-filtration process for initial capture of a monoclonal antibody product using a four-stage countercurrent hollow fiber membrane washing step, Biotechnology and Bioengineering, n/a (2023).

- [15] C. Buchholz, L.F. Reichart, F. Surfaro, R. Maier, F. Zhang, A. Gerlach, F. Schreiber, Kinetics of HSA crystallization and its relationship with the phase diagram, Journal of Crystal Growth, 603 (2023) 126959.
- [16] M. Minervini, A.L. Zydney, Effect of module geometry on the sustainable flux during microfiltration of precipitated IgG, Journal of Membrane Science, 660 (2022) 120834.
- [17] R. Maier, M.R. Fries, C. Buchholz, F. Zhang, F. Schreiber, Human versus Bovine Serum Albumin: A Subtle Difference in Hydrophobicity Leads to Large Differences in Bulk and Interface Behavior, Crystal Growth & Design, 21 (2021) 5451-5459.
- [18] R. Maier, G. Zocher, A. Sauter, S. Da Vela, O. Matsarskaia, R. Schweins, M. Sztucki, F. Zhang, T. Stehle, F. Schreiber, Protein Crystallization in the Presence of a Metastable Liquid–Liquid Phase Separation, Crystal Growth & Design, 20 (2020) 7951-7962.
- [19] M.d.C. Pons Royo, J.-L. Beulay, E. Valery, A. Jungbauer, P. Satzer, Mode and dosage time in polyethylene glycol precipitation process influences protein precipitate size and filterability, Process Biochemistry, 114 (2022) 77-85.
- [20] M. Martinez, G. Mannall, M. Spitali, E.L. Norrant, D.G. Bracewell, Reactor design for continuous monoclonal antibody precipitation based upon micro-mixing, Journal of Chemical Technology & Biotechnology, 97 (2022) 2434-2447.
- [21] E.P. Byrne, J.J. Fitzpatrick, L.W. Pampel, N.J. Titchener-Hooker, Influence of shear on particle size and fractal dimension of whey protein precipitates: implications for scale-up and centrifugal clarification efficiency, Chemical Engineering Science, 57 (2002) 3767-3779.
- [22] J.D. Lee, S.H. Lee, M.H. Jo, P.K. Park, C.H. Lee, J.W. Kwak, Effect of coagulation conditions on membrane filtration characteristics in coagulation Microfiltration process for water treatment, Environmental Science and Technology, 34 (2000) 3780-3788.
- [23] S.A. Lee, A.G. Fane, R. Amal, T.D. Waite, The effect of floc size and structure on specific cake resistance and compressibility in dead-end microfiltration, Separation Science and Technology, 38 (2003) 869-887.
- [24] N.J. Greenfield, Using circular dichroism spectra to estimate protein secondary structure, Nature Protocols, 1 (2006) 2876-2890.
- [25] M.X. Yang, B. Shenoy, M. Disttler, R. Patel, M. McGrath, S. Pechenov, A.L. Margolin, Crystalline monoclonal antibodies for subcutaneous delivery, Proceedings of the National Academy of Sciences, 100 (2003) 6934-6939.
- [26] R.F. Susanti, Y.S. Han, J. Kim, Y.H. Lee, R.G. Carbonell, A new strategy for ultralow biofouling membranes: Uniform and ultrathin hydrophilic coatings using liquid carbon dioxide, Journal of Membrane Science, 440 (2013) 88-97.
- [27] W. Ma, S. Rajabzadeh, A.R. Shaikh, Y. Kakihana, Y. Sun, H. Matsuyama, Effect of type of poly(ethylene glycol) (PEG) based amphiphilic copolymer on antifouling properties of copolymer/poly(vinylidene fluoride) (PVDF) blend membranes, Journal of Membrane Science, 514 (2016) 429-439.
- [28] A.L. Zydney, C.K. Colton, A concentration polarization model for the filtrate flux in cross-flow microfiltration of particulate suspensions, Chemical Engineering Communications, 47 (1986) 1-21.